CHAPTER 5

Performance optimization

In this chapter, mathematical models are developed to perform parametric investigation and optimization of the CO_2 cycle parameters for best possible performance, which was limited in the experimental investigation (Chapter 4). The major contribution of this chapter work is to perform simultaneous optimization of CO_2 trans-critical refrigeration system in terms of both high side pressure and gas cooler face velocity. Parametric investigation of a CO_2 refrigeration system with and without IHX is carried out using a detailed physics-based model and with an Artificial Neural Network (ANN) model trained from experimental input-output data recorded in Chapter 4.

The models are essentially used to predict the energy efficiency (COP) for various working conditions. Evaporation temperature, ambient temperature, gas cooler pressure and air velocity over the gas cooler are chosen as input parameters to predict COP. The physics-based model is an integration of individual models of cycle components of the refrigeration test rig. This include empirical correlation for compressor, finite difference-based model for gas cooler as well as for the IHX and thermodynamic input output-based model for expansion valve and evaporator. A set of experimentally obtained values of COP and corresponding evaporator temperature, gas cooler pressure, air velocity across gas cooler and ambient temperature, as discussed in Chapter 4, are taken as training data for the ANN.

The trained and validated ANN model is then utilized to predict optimal high side pressure as well as gas cooler face velocity for the varying ambient and evaporation conditions to achieve best possible COP. The proposed methodology is deemed suitable for design and testing of control system for maximization of energy efficiency.

5.1 Physics based model

Physics based models are widely employed to simulate as well as to optimize the performance of refrigeration system. This section presents integration of individual models of cycle components of the refrigeration system including compressor, air-cooled gas cooler, double pipe IHX, expansion valve and evaporator. This include empirical correlation for compressor, finite difference-based model for gas cooler as well as for IHX and thermodynamic input output-based model for expansion valve and evaporator. Geometry and specifications of the components are discussed in Chapter 4, under section 4.1. Component-wise modelling of the CO_2 trans-critical refrigeration setup as well as data reduction is described here.

5.1.1 Compressor

The semi-hermetic reciprocating compressor used in the experimental setup is modelled assuming irreversible adiabatic process inside the compressor. Simplified equations for volumetric and isentropic efficiency in terms of evaporation temperature and gas cooler pressure are obtained from the compressor manufactures data. The volumetric efficiency is given by equation (5.1), while the state properties of the refrigerant at inlet is used to compute the mass flow rate, using equation (5.2). The isentropic efficiency of the compressor is modelled with equation (5.3) and the same is utilized to calculate the compressor input power. Equation (5.1) and equation (5.2) are derived using regression based on manufacturer data (Bitzer, 2016) and are valid within gas cooler pressure range from 8 MPa to 11 MPa and evaporation temperature from -10°C to 10°C.

$$\eta_v = 1.18305 + (0.002009 \cdot T_e) - (0.5720 \cdot p_{gc}) - (0.000168 \cdot T_e \cdot T_e) + (0.15 \cdot p_{gc} \cdot p_{gc}) + (0.0043 \cdot T_e \cdot p_{gc}) \quad (5.1)$$

$$\dot{m}_r = \eta_v \cdot \rho_r \cdot V_s \quad (5.2)$$

$$\eta_{is} = (-0.011711 \cdot T_e) + (1.5220 \cdot p_{gc}) + (0.005476 \cdot T_e \cdot T_e) - (0.88 \cdot p_{gc} \cdot p_{gc}) + (0.0134 \cdot T_e \cdot p_{gc}) - (0.0147 \cdot T_e \cdot T_e \cdot p_{gc}) - (0.01 \cdot T_e \cdot T_e \cdot p_{gc} \cdot p_{gc}) \quad (5.3)$$

5.1.2 Gas cooler

The geometry of the finned tube gas cooler is shown in Fig. 4.5, while the actual dimensions of the physical setup are listed in Table 4.2. The mass, momentum and energy conservation for both air and refrigerant side are modelled separately using a finite difference scheme. An elemental grid having dimension of as Δx_i, Δx_j and Δx_k in i, j & k direction, as shown in Fig. 5.1 is made. The tubes are parallel to i direction, while air flows in k directions and j-k is the plane of fins. A one-dimensional heat and fluid flow model is constructed and solved for one grid, and the solution is extended for entire geometry element by element. Major assumptions made for the analysis are (a) thermal equilibrium at each grid, (b) heat conduction within fins and along the pipe axis neglected, (c) homogenous distribution of air flow, (d) thermal resistance neglected at the joint of pipe and fins.

The mass, momentum and energy conservation equations for refrigerant flow are discretised using finite difference scheme for a grid from coordinates (i, j, k) to (i+1, j, k), as shown in equation (5.4) to equation (5.6). The pressure drop in the refrigerant side is calculated using equation (5.7). An additional pressure drop is considered for U bends at the end of each tube. In equation (5.7), φ is the friction coefficient and is calculated using equation (5.8) (Gupta and Dasgupta, 2014).

$$(\dot{m}_r)_{(i+1,j,k)} = (\dot{m}_r)_{(i,j,k)} \quad (5.4)$$

$$\frac{1}{A_{inner}}\left[(\dot{m}_r \cdot V_r)_{(i+1,j,k)} - (\dot{m}_r \cdot V_r)_{(i,j,k)}\right] + \Delta p_r = 0 \quad (5.5)$$

$$\frac{\left[(\dot{m}_r \cdot V_r)_{(i+1,j,k)} - (\dot{m}_r \cdot V_r)_{(i,j,k)}\right]}{\Delta x_i} + \frac{\pi \cdot d_{outer} \cdot \dot{q}}{\dot{m}_r} = 0 \tag{5.6}$$

$$\Delta p_r = \frac{\varphi \cdot G^2 \cdot \Delta x_i}{2 \cdot \rho_r \cdot d_{inner}} \tag{5.7}$$

$$\varphi = \frac{1}{[0.79 \ln(Re) - 1.64]^2} \tag{5.8}$$

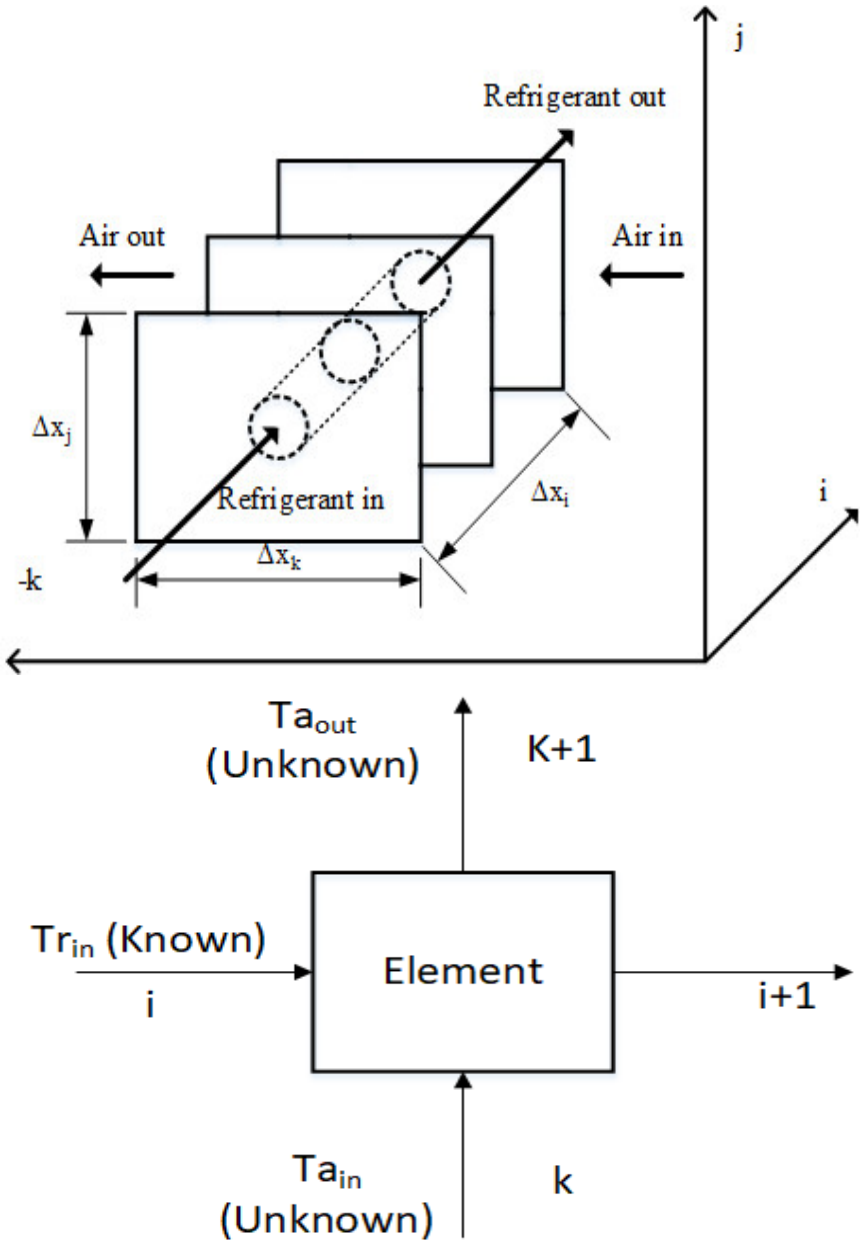

Fig. 5.1 Grid for gas cooler with flow directions

The refrigerant side heat transfer coefficient is calculated using equation (5.9). Nusselt number (Nu) in the equation (5.10) is computed as an average value based on thermo-physical properties at the wall and bulk temperature (Pitla et al., 2002). Wall and bulk temperatures are evaluated iteratively by initially assuming them as equal to the temperature of refrigerant and air respectively. Nu_{bt} and Nu_{wt} are individually calculated using equation (5.11) (Gnielinski, 1976).

$$\alpha_r = \frac{Nu \cdot k_{bt}}{d_{inner}} \tag{5.9}$$

$$Nu = \left[\frac{Nu_{wt} + Nu_{bt}}{2}\right] \cdot \left[\frac{k_{wt}}{k_{bt}}\right] \tag{5.10}$$

$$Nu_{(wt,bt)} = \frac{\frac{\varphi_{(wt,bt)}}{8} \cdot \left(Re_{(wt,bt)} - 1000\right) \cdot Pr_{(wt,bt)}}{12.7 \cdot \sqrt{\frac{\varphi_{(wt,bt)}}{8}} \cdot \left(Pr_{(wt,bt)}^{\frac{2}{3}} - 1\right) + 1.07} \tag{5.11}$$

Following effectiveness – NTU method, the heat transfer in the air side at grid points are calculated using equation (5.12). In equation (5.12), ε is the effectiveness of the grid and the same is calculated using the equations (5.13) and equations (5.14) for the value of $C_{max} = C_h$ and $C_{min} = C_h$, respectively.

$$\dot{Q}_a = \varepsilon \cdot C_{min} \cdot \left(T_r(i,j,k) - T_a(i,j,k)\right) \tag{5.12}$$

$$\varepsilon = 1 - e^{(-\gamma \cdot C_r)};\ \gamma = 1 - e^{\left(-\left({}^{U_o \cdot A}/_{C_{max}}\right)\right)};\ C_r = {}^{C_{max}}/_{C_{min}} \tag{5.13}$$

$$\varepsilon = C_r \cdot \left(1 - e^{\left(-\gamma \cdot \left({}^{1}/_{C_r}\right)\right)}\right);\ \gamma = 1 - e^{\left(-\left({}^{U_o \cdot A}/_{C_{min}}\right)\right)} \tag{5.14}$$

The heat transfer coefficient in air-side is calculated using equation (5.15) and (5.16) (Incropera and DeWitt, 1996). The fan power, as measured experimentally (Chapter 4, article

4.4) for the different air flow velocities, are used to formulate a mathematical expression for fan power in terms of air velocity, as in equation (5.17), and the same is used for calculating pressure drop in air-side, as in equation (5.18).

$$Nu_a = 0.683 \cdot Re_a^{0.466} \cdot Pr_a^{0.33} \tag{5.15}$$

$$\alpha_a = \frac{Nu_a \cdot k_{bt}}{d_{eq}} \tag{5.16}$$

$$\dot{W}_f = 21.814 \cdot (V_a)^{2.5142} \tag{5.17}$$

$$\Delta p_a = \dot{W}_f \cdot V_a \cdot A_a \tag{5.18}$$

The overall heat transfer coefficient for the gas cooler is calculated using equation (5.19), where $\sum R_{ct}$ is the conduction resistance through tube wall and fins. The overall fin surface efficiency (η_{os}) required for equation (5.19) is calculated using equation (5.20) (Wang et al., 1999). Heat balance between air and refrigerant side for each grid is calculated using equation (5.21).

$$U_o \cdot A = \left(\frac{1}{\alpha_a \cdot \eta_{os} \cdot A_a} + \sum R_{ct} + \frac{1}{\alpha_r \cdot A_{inner}}\right) \tag{5.19}$$

$$\eta_{os} = \left(1 - \frac{A_{fin}}{A_a}\left(1 - \eta_{fin}\right)\right) \tag{5.20}$$

$$\dot{Q}_a = U_o \cdot A(i,j,k)[T_r(i,j,k) - T_a(i,j,k)] \tag{5.21}$$

An iterative method is used for simultaneously solving the air and refrigerant side equations, i.e. for i+1 and k+1 grids, respectively. The gas cooler is counter cross-flow type, and only one temperature out of four is known for an element as shown in Fig. 5.1. Hence one or

more temperatures are to be assumed, consequently, air temperature at gas cooler outlet is assumed. The discretised equations are solved iteratively to find the temperature of refrigerant at gas cooler outlet with error converging to the order of 10^{-3}.

5.1.3 IHX

The double pipe IHX, as shown in schematic diagram, Fig. 4.6, is modelled likewise the modelling procedure of the gas cooler, but both the fluids are CO_2 here. The specific details for the IHX in experimental setup is listed in Table 4.3. CO_2 at high pressure from the gas cooler is fed into the inner tube of IHX, while the low-pressure CO_2 from the evaporator flows through the outer tube of the IHX.

The grid elements considered while modelling IHX is shown in Fig. 5.2. The refrigerant side heat transfer coefficients are calculated for both cold and hot streams using equations (5.8) to equation (5.11), while the pressure drops in both streams are calculated using equation (5.7). Perfectly insulated IHX is assumed, implying thereby heat lost from the hot side is equal to heat gained by cold side.

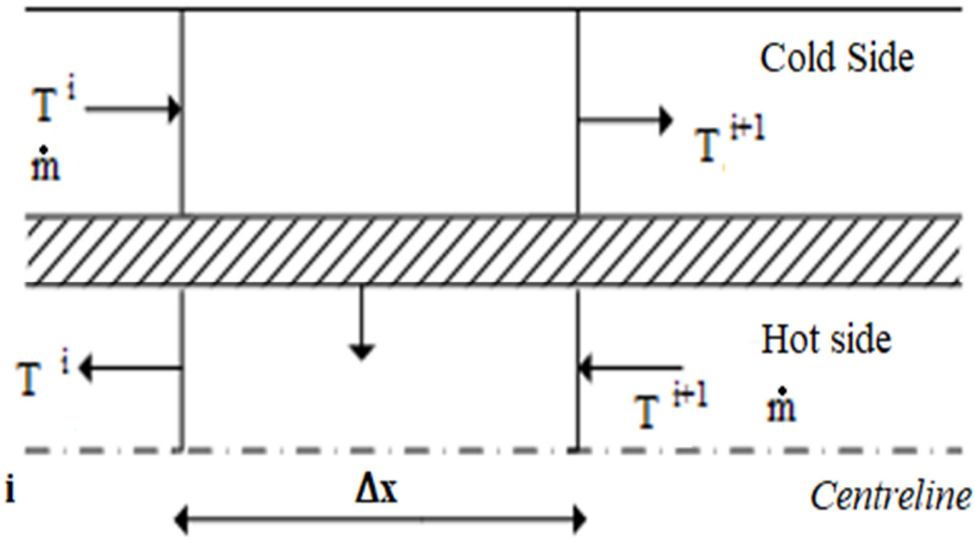

Fig. 5.2 Grid for IHX with flow directions

5.1.4 Expansion valve

A manual expansion valve is modelled using thermodyanmic state point properties. Expansion process is modelled ensuring pressure drop within IHX as well as in the expansion valve. Enthalpy at the exit of IHX (higher pressure side) is calculated at the temperature and pressure calculated through simulation. The enthalpy at evaporator inlet is computed as a state point property at temperature and pressure predicted by simulation at outlet of expansion valve.

5.1.5 Evaporator

The geometry of the evaporator is shown in Fig. 4.9 and its specifications are given in Table 4.4. For operation under various conditions during the experimental study, the useful superheating at evaporator exit is controlled by simultaneously adjusting refrigerant charge and the setting of the manually adjustable expansion valve. Adequate care is taken to maintain superheating at the evaporator exit, and no two-phase flow is permitted. The evaporator is modelled considering 10 K of superheating as the same is achieved for all experimental runs.

5.1.6 Energy efficiency (COP) calculations

Compressor input power, refrigeration capacity and COP are calculated using equations (5.22) to equation (5.24).

$$\dot{W}_c = \dot{m}_r \cdot \left(h_{r,out} - h_{r,in}\right)_c \tag{5.22}$$

$$\dot{RE}_r = \dot{m}_r \cdot \left(h_{r,out} - h_{r,in}\right)_e \tag{5.23}$$

$$COP = \frac{\dot{RE}_r}{\left(\dot{W}_c + \dot{W}_f\right)} \tag{5.24}$$

The simulation is carried out in MATLAB platform by combining the individual component models, and REFPROP 9.0 (Lemmon et al., 2002) is used for obtaining air and refrigerant side properties. The iterative algorithm is illustrated in Fig. 5.3.

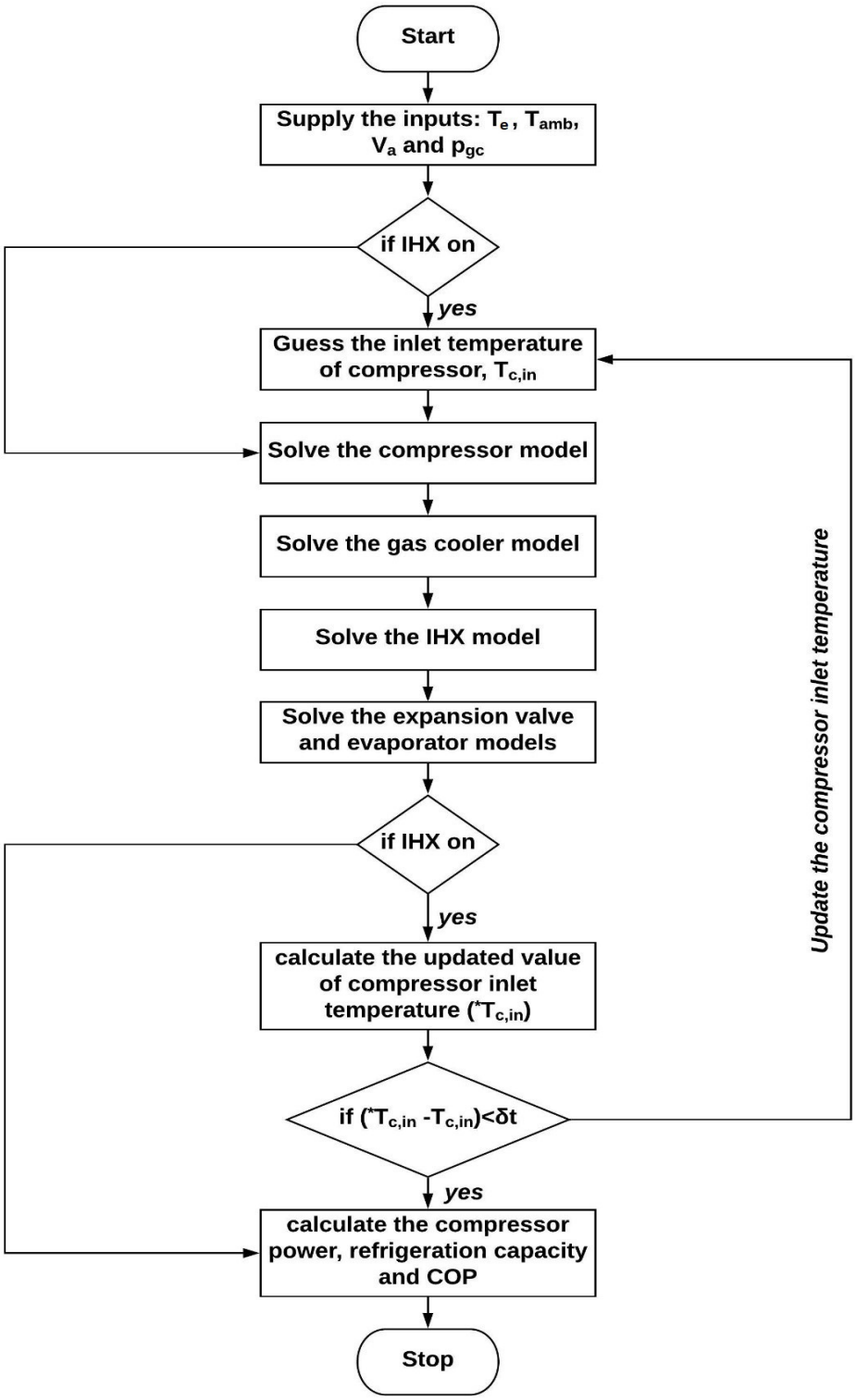

Fig. 5.3 Numerical algorithm to solve physical model of CO_2 trans-critical refrigeration system with and without IHX

5.2 Artificial Neural Network (ANN) model

MATLAB toolbox is used to train and validate the ANN based model. An ANN captures a collection of distributed parameters from input-output data of a process through an iterative training algorithm (Dasgupta et al., 2001) to construct an input-output based model. The smallest unit in an ANN is a neuron, which can be an individual microprocessor. Each neuron in a trained ANN produces an output, when activated with an input stimulus beyond a threshold.

The motivation for implementation of an ANN is to reduce extent of experimentation which is costly and time-consuming. Wu et al., (2008) proposed an ANN to predict the performance of a gas cooler in a CO_2 heat pump. They discussed the parametric analysis of gas cooler based on the trained ANN. Belman-Flores et al., (2015) presented an ANN-based modelling of a reciprocating compressor for a refrigeration system. They reported that the trained ANN could predict the performance with less than ±1% mean relative error, whereas the error for the physics-based model was up to ±10%. Wang et al., (2016) presented an ANN based model of a hybrid ejector air-conditioning system. They compared results from three types of neural networks to the of experimental findings and concluded that a multi-layer perceptron (MLP) type network is best suited for this purpose. Some other studies propose use of ANN to predict the performance of a CO_2 based scroll expander (Singh et al., 2017) and heat exchanger (Son et al., 2018) as well as to assess second law efficiency of the system (Belman-Flores et al. 2018).

A common ANN architecture has an input layer, an output layer and may have several hidden layers. The ANN architecture used in this study (Fig. 5.4), is composed of one hidden layer with sufficient neurons. The number of hidden neurons is varied within range 6 to 13 iteratively with Logsig transfer function (Belman-Flores et al., 2015) and a model is established

to avoid overfitting, while maintaining the desired accuracy (10^{-3}). The learning rate and the number of epochs for the model considered are 0.01 and 1000, respectively. Based on the error coefficients, minimum eight hidden neurons are considered for the prediction of COP for both cycles with and without IHX. The input parameters are evaporation temperature, ambient temperature, gas cooler pressure and air velocity over the gas cooler, while the output is COP.

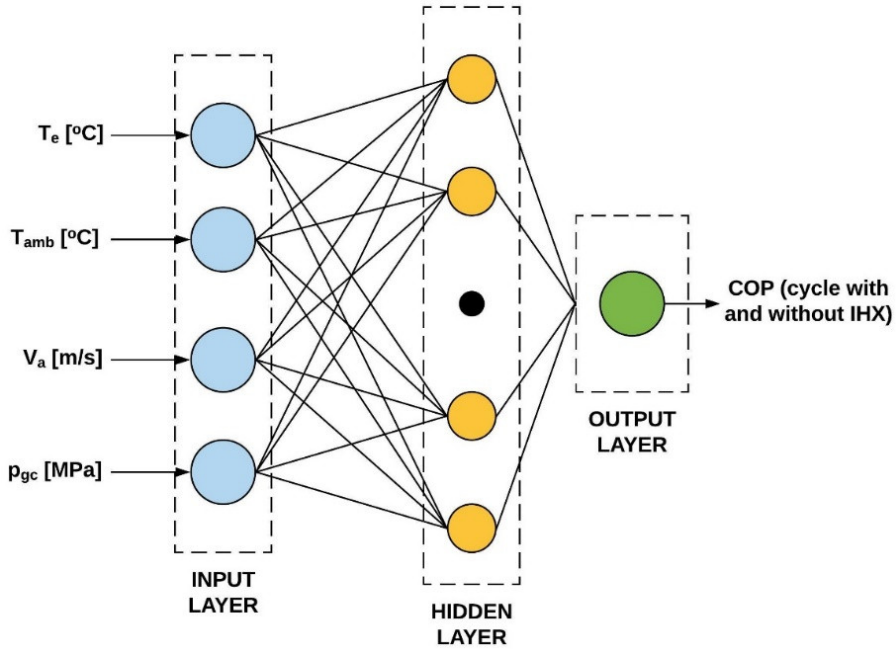

Fig. 5.4 ANN architecture for the output parameters

A total of 156 experimental input-output data points for the basic and IHX cycle are divided into two sets: 80% in training and remaining data in validation sets. The modelling of ANN in this article starts with normalising the data set in the interval 0.1 to 0.9, followed by training of ANN based on feed forward back propagation technique employing the Levenberg–Marquardt training algorithm, the neurons are seeded with initial weights and thresholds. The output from the hidden neurons are similarly scaled back. The statistical coefficient namely, mean relative error (MRE) and root mean square error (RMSE) as defined as in equation (5.25)

and (5.26) are computed. The flowchart for training the ANN is shown in Fig. 5.5 and the statistical coefficients of the trained neurons are listed in Table 5.1.

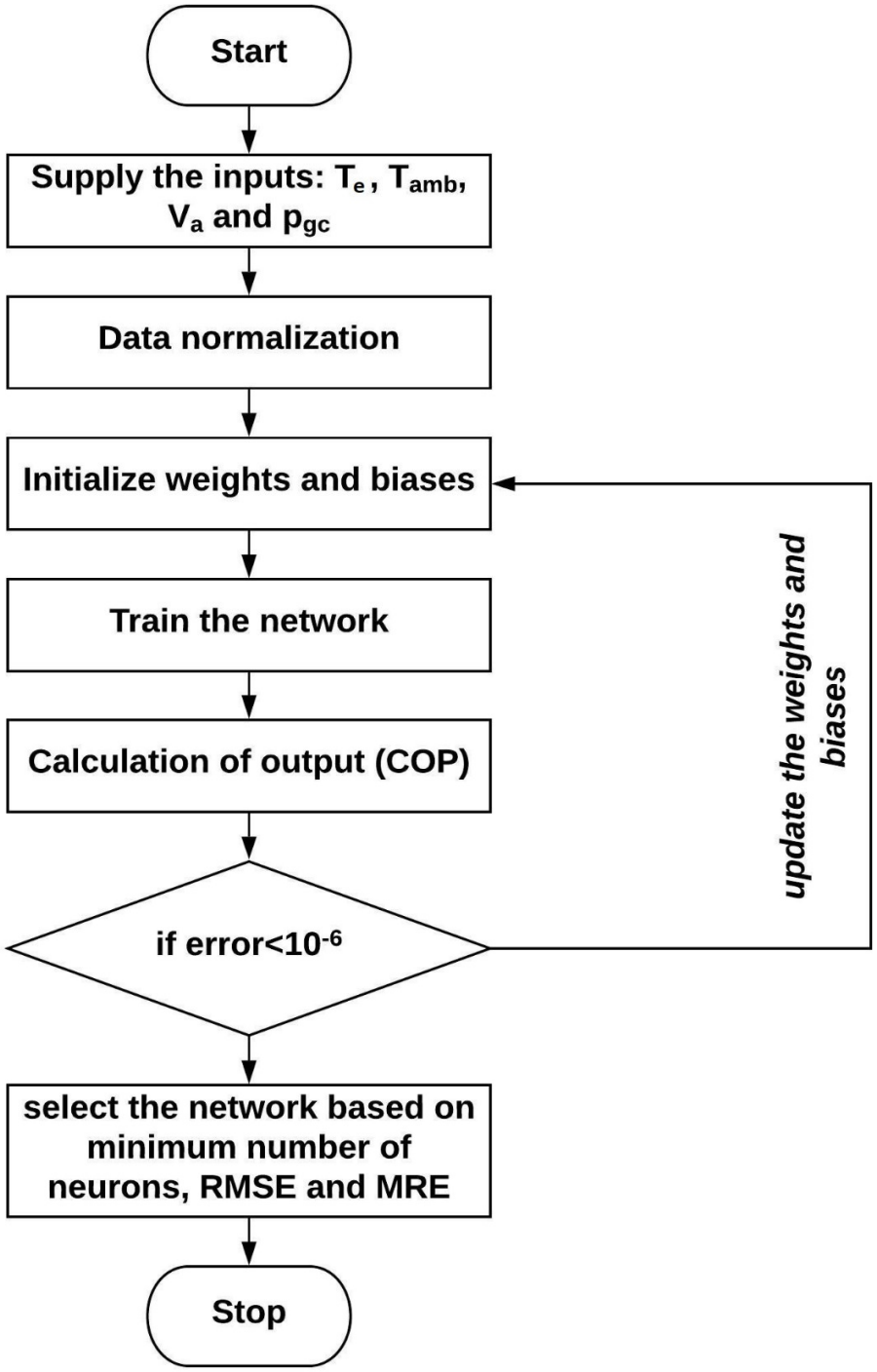

Fig. 5.5 Flow chart for training of ANN

$$mre = \frac{1}{N}\sum_{k=1}^{N}\left|\frac{u_{ANN,k} - u_{experimental,k}}{u_{experimnetal,k}}\right| \times 100\% \quad (5.25)$$

$$rmse = \sqrt{\frac{1}{N}\sum_{k=1}^{N}\left(\frac{u_{ANN,k} - u_{experimental,k}}{u_{experimnetal,k}}\right)^2} \quad (5.26)$$

Table 5.1 Statistical coefficient obtained during training process of ANN

No. of neurons	Cycle with IHX		Cycle without IHX	
	RMSE (-)	***RME %***	***RMSE (-)***	***RME %***
4	0.151	1.782	0.143	1.612
5	0.128	1.512	0.125	1.321
6	0.102	1.015	0.109	1.421
7	0.095	1.235	0.087	1.021
8	*0.083*	*0.417*	*0.074*	*0.401*
9	0.084	0.895	0.065	0.357

5.3. Model validation

The COP prediction using physics-based model as well as trained ANN, are plotted against the reference experimental data set collected in this study (78 data points each for cycle with and without IHX). Fig. 5.6 (a) for cycle with IHX and Fig. 5.6 (b) for cycle without IHX, shows comparison of error coefficients for both models. The error level is nearly same for cycle with and without IHX. It is observed from the Fig. 5.6 that the rmse and mre in predictions using ANN model are 0.0074 and 0.401%, respectively. While the rmse and mre for the physics-based model are 0.1145 and 7.011%, respectively. Fig. 5.6 also depicts the mse in predictions using ANN model trained with fewer training data sets (abbreviated as ANN* and marked by green line).

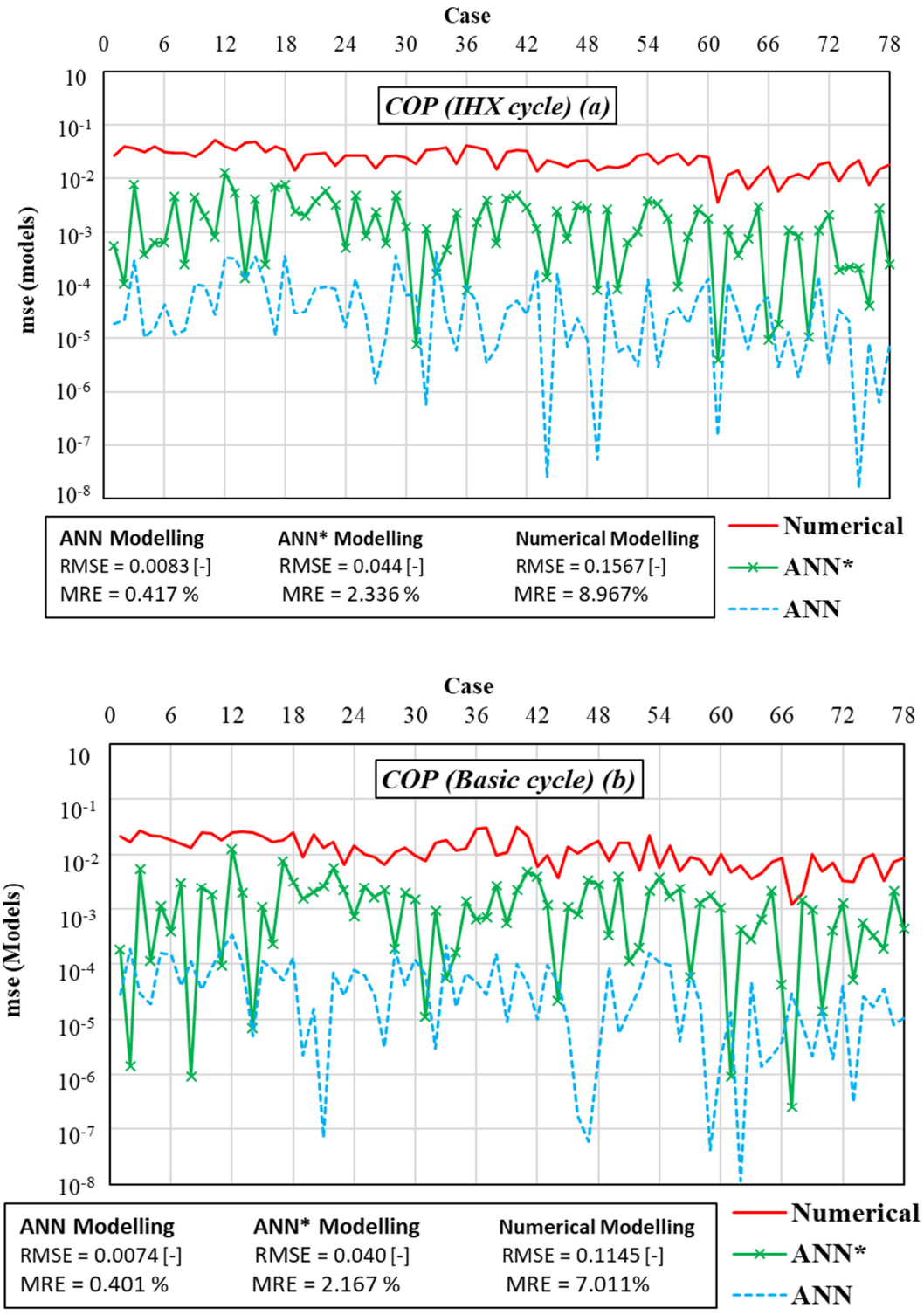

Fig. 5.6 Comparison of mse for ANN and physical models for cycle with (a) with IHX (b) without IHX.

It is observable that, with 50% fewer training data points, the error level in predictions using ANN* increases to 2.33% but is still useful. Prediction of optimum operating condition from trained ANN and control system implementation can become a lot easier if ANN can be systematically trained with lesser experimental data and the same may be explored in future. Comparatively high error in predictions using physics-based model is attributed to the various assumptions made, such as neglecting the heat losses and the pressure drop for the components as well as for the pipeline. Non-incorporation of detailed model for some components like receiver, accumulator and piping also contributed to error. Further, evaporator load simulation and ambient temperature simulation are absent in the model. The ANN model is further explored for optimising the critical operating parameters as the same is found to better follow the experimental observations.

5.4 Parametric optimization using trained ANN model

The developed and validated ANN model is utilised to perform a parametric investigation and optimization. Among the many critical parameters, affecting the CO_2 cycle performance in the trans-critical region, the high side pressure and gas cooler face velocity are focused. The simulated study is extended to optimize the CO_2 cycle performance. The upper and lower limit of high side pressure and gas cooler face velocity are kept in accordance with the experimental study. For optimization of performance, a high side pressure range from 80 bar to 110 bar is considered, while the face velocity range within 1 $m \cdot s^{-1}$ to 3 $m \cdot s^{-1}$. Maintaining gas cooler face velocity as 1 $m \cdot s^{-1}$, the effect of high side pressure on COP in trans-critical region is investigated using simulation based study. The results obtained using physics based model and ANN are plotted in Fig. 5.7 and Fig. 5.8, respectively, for evaporation temperature of -5ºC at varying ambient conditions. In both Fig. 5.7 and Fig. 5.8, the solid line represents predictions from

simulation study while the dotted line depicts experimental observations. It may be concluded from the Fig. 5.7 and Fig. 5.8 that the simulated study is able to capture the trend of COP variation with respect to gas cooler pressure as observable from the trend of experimental data. Predictions from the ANN is closer to experimental observations than that from physics based model.

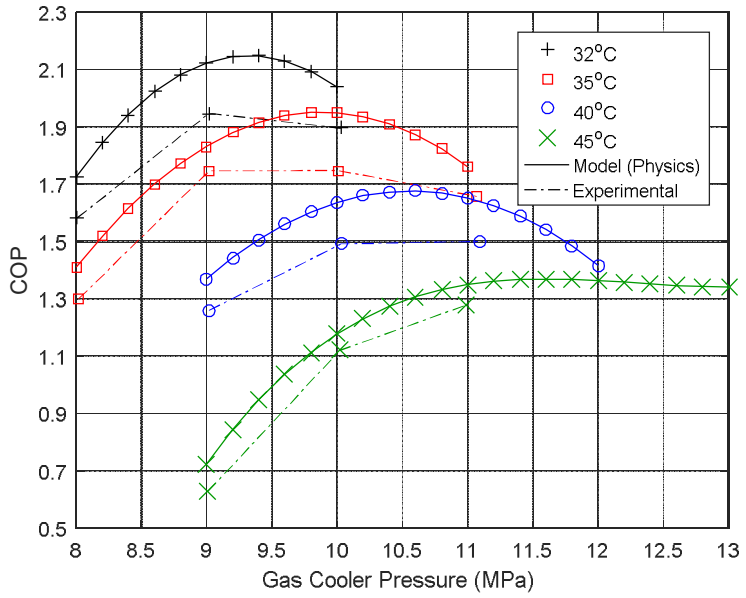

Fig. 5.7 Effect of high side pressure on COP (Physics based model simulation)

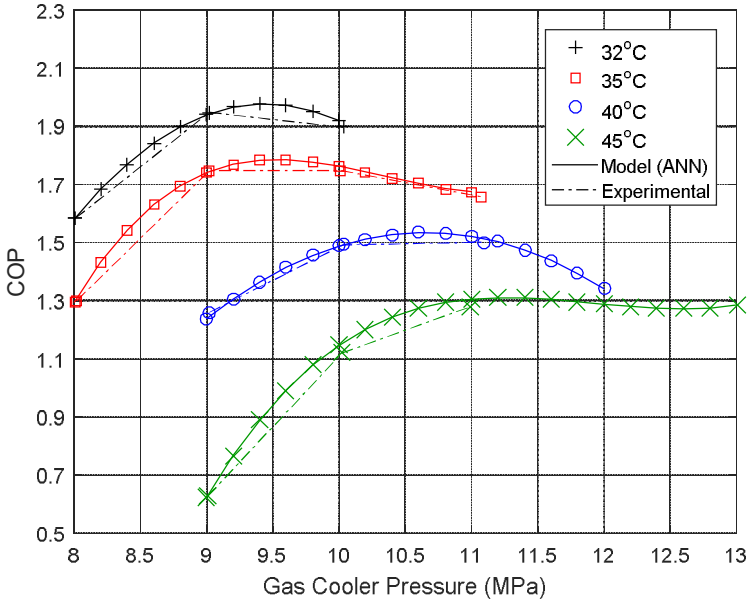

Fig. 5.8 Effect of high side pressure on COP (ANN based model simulation)

As expected, the performance of cycle decreases with increase in ambient temperature. At a particular ambient temperature, with rise in gas cooler pressure, the COP of the system increases, reaches a plateau for a particular gas cooler pressure and then decreases. This is attributed to the fact that with increase in gas cooler pressure both the compressor power and refrigeration capacity increases. However, they have contradictory effect on COP and the rate of increment in refrigeration effect dominates up to a certain gas cooler pressure and beyond that, the rate of increment in compressor power dominates. An elaborate control strategy is therefore, required to operate a CO_2 trans-critical cycle at optimal high side pressure to take advantage of trade-off between the increment in both compressor power and refrigeration capacity.

It can be noted from Fig. 5.7 that the cycle performance in the vicinity of critical point is more sensitive to operating pressure on either side of the optimal set point. At ambient temperature of 32ºC and evaporation temperature of -5ºC, the best possible COP of system is achieved in the narrow range of operating high side pressure, 90 bar to 95 bar. Further, COP of the system tends to deteriorate drastically when the operating high side pressure is outside this optimal range of 90 bar to 95 bar. As ambient temperature increases, the variation of COP with change in gas cooler pressure, tends to become flatter for the region in the close vicinity of optimal gas cooler pressure. That implies performance of a CO_2 trans-critical refrigeration cycle in higher ambient conditions (45ºC) is very less sensitive to operating high side when operated near required optimal value.

Simultaneous optimization of face velocity of gas cooler and high side pressure is attempted for the various ambient and evaporation conditions in CO_2 refrigeration system. The optimization algorithm searches for optimal solution in the defined range. The combined effect

of air velocity over the gas cooler and the high side pressure on COP at ambient temperature of 35°C and evaporation temperature of 0°C are simulated and represented in Fig. 5.9.

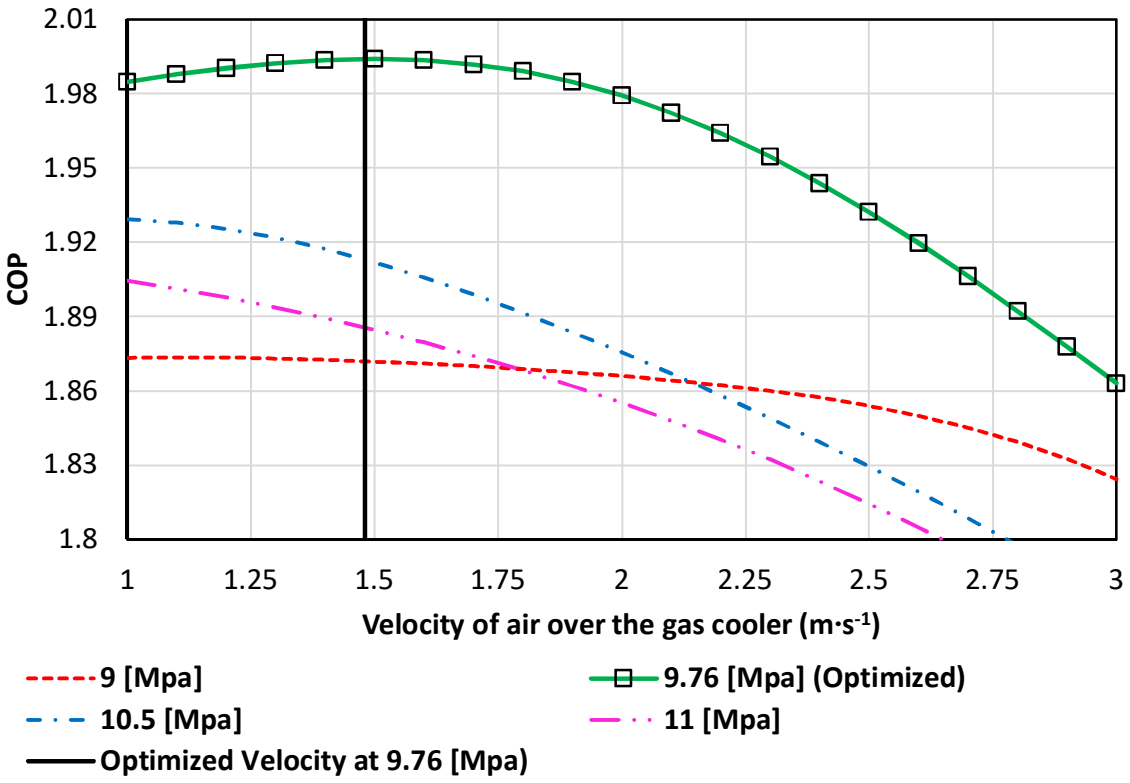

Fig. 5.9 Effect of air velocity over the gas cooler on COP (T_o = 0°C, T_a = 35°C) at various operating gas cooler pressure

As observable from Fig. 5.9 within the range of face velocity ranging from 1 m/s to 2 m/s, COP of the system reaches maxima. Any further, increase in air velocity leads to deterioration in performance of system. This is attributed to the fact that with increase in face velocity, both the gas cooler performance and the fan power consumption increases, but at a different rate. That implies that there is scope of selecting an optimum air velocity. At ambient of 35°C a maximum of 2.314% improvement in COP of the cycle with IHX is possible when the gas cooler is operated at a pressure of 9.76 MPa, and the air-side velocity is kept as 1.48 $m \cdot s^{-1}$. Therefore, it may be concluded that for CO_2 trans-critical system with air cooled gas cooler,

optimization of gas cooler face velocity along with operating high side pressure is necessary and leads to significant improvement in the performance. The obtained optimized parameters, as well as the predicted COP, are listed in Table. 5.2. The percentage improvement with respect to experimental observations are also listed. A possibility of 5.31% improvement in COP is predicted using simulation-based optimization of critical parameters viz high side pressure and air velocity over the gas cooler. which can be established with an automated control system.

Table 5.2 Optimized operating parameters and COP for CO_2 refrigeration system

CO_2 refrigeration system without IHX					
Input				**Output**	
T_e [^oC]	*T_{amb} [^oC]*	*p_{gc} [MPa]*	*V_a [$m \cdot s^{-1}$]*	*COP_{opt}*	*% improvement to COP*
-5	32	9.32	1.54	2.031	5.26
	35	9.61	1.37	1.766	2.29
	40	10.52	1.12	1.491	1.21
	45	11.00	1	1.21	0
0	32	9.39	1.61	2.308	5.31
	35	9.76	1.48	1.996	2.31
	40	10.71	1.14	1.667	1.33
	45	11.00	1	1.35	0
CO_2 refrigeration system with IHX					
-5	32	9.28	1.51	2.047	5.12
	35	9.58	1.35	1.792	2.26
	40	10.47	1.08	1.533	1.01
	45	11.00	1	1.27	0
0	32	9.31	1.59	2.314	5.15
	35	9.74	1.43	2.018	2.28
	40	10.66	1.11	1.703	1.11
	45	11.00	1	1.42	0

5.5 Summary

The performance of CO_2 trans-critical refrigeration system with and without IHX are investigated based on physics-based model and an ANN model. COP is predicted for a set of input parameters which include evaporation temperature, ambient temperature, gas cooler pressure and gas cooler face velocity. Output in terms of COP from both modelling approaches are compared with experimental outcome. The mean relative error is found below ±10% for physics-based model and below ±1% for ANN model. The trained and validated ANN model is further utilized to investigate the effect of change of input parameters, gas cooler pressure and face velocity, on COP to optimize cycle performance. A possibility of 5.31% improvement in COP is predicted based on the optimization of parameters, which can be established with an automated control system.